Overview of HL-2A Recent Experiments

X.R. Duan[1], Yi Liu[1], M. Xu[1], L.W. Yan[1], Y. Xu[1], X.M. Song[1], J.Q. Dong[1], X.T. Ding[1], L.Y. Chen[1], B. Lu[1], D.Q. Liu[1], J. Rao[1], W.M. Xuan[1], Q.W. Yang[1], G.Y. Zheng[1], X.L. Zou[2], Y. Q. Liu[3], W.L. Zhong[1], K.J. Zhao[1], X.Q. Ji[1], W.C. Mao[1], Q.M. Wang[1], Q. Li[1], J.Y. Cao[1], Z. Cao[1], G.J. Lei[1], J.H. Zhang[1], X.D. Li[1], X.Y. Bai[1], J. Cheng[1], W. Chen[1], Z.Y. Cui[1], L. Delpech[2], P.H. Diamond[4], Y.B. Dong[1], A. Ekedahl[2], T. Hoang[2], Y. Huang[1], K. Ida[5], K. Itoh[5], S. Itoh[6], M. Isobe[5], S. Inagaki[6], D. Mazon[2], S. Morita[5], Y. Peysson[2], Z.B. Shi[1], X.G. Wang[7], G.L. Xiao[1], D.L. Yu[1], L.M. Yu[1], Y.P. Zhang[1], C.H. Cui[1], B.B. Feng[1], M. Huang[1], B. Li[1], G.S. Li[1], H.J. Li[1], Qing Li[1], J.F. Peng[1], Y.Q. Wang[1], B.S. Yuan[1], Yong Liu[1] and HL-2A team

[1]Southwestern Institute of Physics, P.O. Box 432, Chengdu 610041, China
[2]CEA, IRFM, F-13108 Saint-Paul-lez-Durance, France
[3]CCFE, Culham Science Centre, Abingdon, Oxfordshire, OX14 3DB, UK
[4]CASS & Department of Physics, UCSD, La Jolla, CA 92093, USA
[5]National Institute for Fusion Science, 322-6 Oroshi-cho, Toki-shi 509-5292, Japan
[6]Research Institute for Applied mechanics, Kyushu University, Kasuga, Kasuga keon 6-1, 816-8580, Japan
[7]Harbin Institute of Technology, Harbin, Hei Long Jiang 150006, China
E-mail contact of main author: duanxr@swip.ac.cn

Abstract. Since the last Fusion Energy Conference,significant progress has been made in the following areas: the first High coupling efficiency of low-hybrid current drive (LHCD) with the Passive-Active Multi-junction (PAM) antenna was successfully demonstrated in H-mode on the HL-2A tokamak; double critical impurity gradients of electromagnetic turbulence were observed in H-mode plasmas; A new pedestal mode, leading an inward particle flux, was observed prior to each ELM onset; Various ELM mitigation techniques have been investigated, including supersonic molecular beam injection (SMBI), impurity seeding, resonant magnetic perturbation (RMP) and low-hybrid wave (LHW);The ion internal transport barrier was observed in the neutral beam injection (NBI) heated plasmas; Neoclassical tearing modes (NTMs) driven by the transient perturbation of local electron temperature during the non-local thermal transport events have been observed, and a new-type non-local transport triggered by the ion fishbone was found; Long-lasting runaway electron plateau was achieved after argon injection and the runaway current was successfully suppressed by SMBI; It was found that low-n Alfvenic ion temperature gradient (AITG) modes can be destabilized in ohmic plasmas even with weak magnetic shear and low pressure gradients; For the first time, the synchronization of geodesic acoustic mode (GAM) and magnetic fluctuations was observed in the edge plasmas, revealing the frequency entrainment and phase lock; Spatiotemporal features of zonal flows have been studied by using multi-channel correlation Doppler reflectometers.

1. Introduction

In recent years the HL-2A tokamak programme has been aimed to address the key physic issues relevant to ITER. In order to achieve the goal, many subsystems such as auxiliary heating and diagnostic systems, have been upgraded or developed. The newly developed 3.7 GHz low-hybrid current drive (LHCD) system in HL-2A consists of a Passive-Active Multi-junction (PAM) launcher [1]. The first LHCD experiments with the PAM in H-mode [2]

were carried out. The coupled LH power reached 900 kW in H-mode plasmas. One H-mode discharge is shown in Fig. 1. The LH power can be coupled at large plasma-launcher gap (e.g. 11cm gap for 0.5MW coupled power), and assist in triggering and sustaining H-modes. Some advanced diagnostic systems have been developed and upgraded, including a multi-channel HCOOH laser interferometer and polarimeter [3,4] for density and Faraday rotation measurement, a 384-channel electron cyclotron emission imaging (ECEI) system for 2D electron temperature fluctuation measurement[5], a multi-channel correlation Doppler backscattering reflectometer (DBS) for poloidal rotation and turbulence measurement [6], a Doppler coherence imaging system for toroidal rotation measurement, a high-frequency magnetic probe array for detecting high mode-number (m/n=20/30) MHD instabilities [7], a wide-angle infrared (IR) periscopes diagnostic for observing plasma wall interaction in the main chamber, etc. A variety of fuelling techniques, such as massive gas injection (MGI), gas mixture supersonic molecular beam injection (SMBI), have been developed or improved. These upgrades greatly enhanced the capability for the study of advanced plasma physics on the machine.

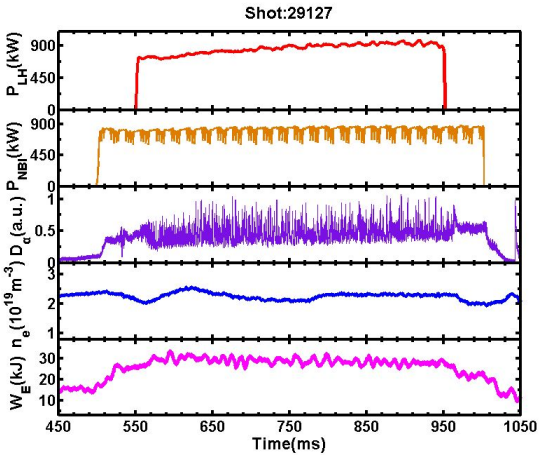

Figure 1. Time evolution of main parameters for the plasmas with coupled LHW power reaching 900 kW in H-mode.

The achieved operation parameters on HL-2A (R = 1.65 m, a = 0.4 m) are as what follows. The toroidal magnetic field B_t=2.7 T, plasma current I_p = 430 kA, discharge duration 6.1 s, line-averaged electron density n_e=6×10^{19}cm^{-3}，electron and ion temperatures T_e = 5 keV and T_i = 2.8 keV, respectively. Since the last FEC, the experiments on HL-2A tokamak have been focused on the investigations on H-mode physics, ELM mitigation and control, core plasma transport, MHD and energetic particle physics, and edge turbulence. In particular the observation of double critical impurity gradients of electromagnetic turbulence [8], role of quasi-coherent mode in pedestal dynamic [9], ELM mitigation and control by SMBI [10], impurity seeding, resonant magnetic perturbation (RMP) and low-hybrid wave (LHW), observation of ion internal transport barrier [11], non-local heat transport induced by fishbone [12], turbulence transition between trapped electron mode and ion temperature gradient mode [13], interplay between neoclassic tearing mode and non-local transport [14], impurity transport [15], mitigation of runaway current with SMBI [16], observation of Alfven ion temperature gradient mode and internal kink mode [17], interaction between magnetic island and geodesic acoustic mode (GAM) [18], and zonal flows measured by Doppler reflectometry [19]. The major experimental results are reviewed in this paper while the details are described in corresponding references.

This paper is arranged as the following. H-mode physics results are given in section 2;ELM mitigation and control by various methods are summarized in section 3; Core plasma transport studies are presented in section 4; MHD and energetic particle physics are discussed in section 5; Edge turbulence studies are shown in section 6; Section 7 is a brief summary.

2. H-mode physics

In HL-2A, recent experiments in the area of H-mode physics were focused on the study of pedestal dynamics and underlying instabilities. The impact of impurity on pedestal dynamics and instabilities has been investigated recently [20]. It was found that a broadband electromagnetic turbulence could be excited by impurities in the H-mode plasmas, and double critical impurity gradients of the turbulence were observed [8]. In pedestal region, a new pedestal quasi-coherent mode (QCM), which led an inward particle flux, was observed prior to each ELM onset. It contributes significant additional density and its gradient/pressure gradient increase and may trigger the ELM onset [9].The origin of the oscillating radial electric field in intermediate confinement phase (I-phase) and its roles in the transition has been studied.

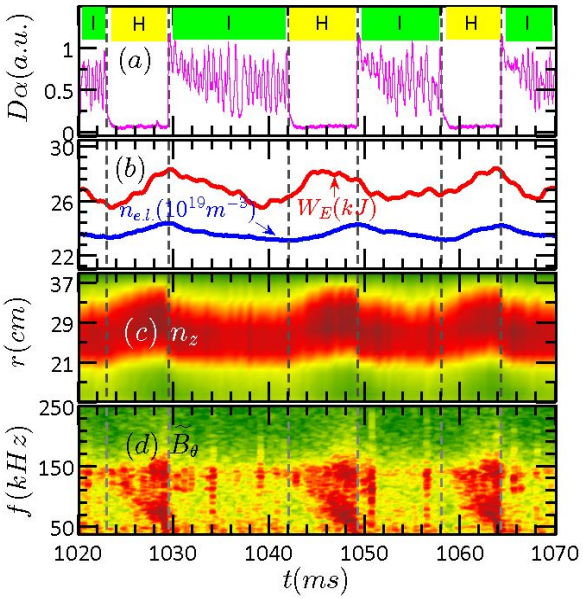

Figure 2. (a)Divertor Da signal, (b) inner stored energy and line-averaged electron density, (c) effective impurity density, (d) spectrogram of magnetic fluctuations.

2.1 Double Impurity Critical Gradients for Electromagnetic Turbulence Excitation

In HL-2A, the impact of impurity on pedestal dynamics and instabilities has been investigated recently. Experimental results have shown that, during the H-mode phase, the impurity was gradually accumulated at the edge plasma region (Fig.2c), and a broadband (frequency of 50-150kHz) electromagnetic turbulence was observed from the spectrogram of magnetic fluctuations (Fig.2d). The excitation of the turbulence was strongly correlated to the accumulation of impurity at the plasma peripheral region. Then the ELM-free phase was ended with the onset of an ELM-like event. After that, the impurity is immediately exhausted, and the plasma transits into the I-phase, with the generation of electrostatic turbulence modulated by limit cycle oscillations. With the gradually increasing pedestal pressure

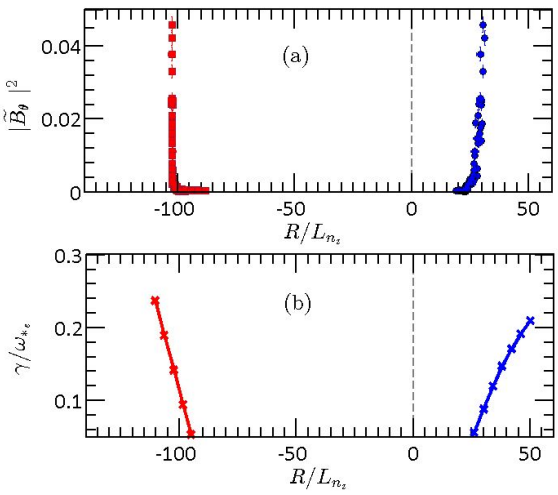

Figure 3. (a) Experimental result: the relation between the intensity of electromagnetic turbulence and the normalized impurity density gradient, (b) simulation results by the HD7 code for electromagnetic turbulence: the normalized linear growth rate of electromagnetic turbulence versus the normalized impurity density gradient.

gradient during the I-phase, the plasma returns to the H-mode regime. It suggests that the electromagnetic turbulence plays a key role in the cyclic transitions between the I-phase and H-mode.

Figure 3a illustrates the measured intensity of the electromagnetic turbulence as a function of normalized impurity density gradient in positive and negative gradient regions. Double impurity critical gradients have been observed for the excitation of the turbulence [9]. The critical value of $|R/L_{nz}|$ in positive gradient region is much lower than that in the negative region. The effects of the carbon impurity ions on electromagnetic turbulence have been studied with a gyrokinetic code HD7. The simulation result in Fig.3b also shows double critical gradients in R/L_{nz}. For the turbulence excitation mechanism, the mode is driven by the impurity density gradient in the positive R/L_{nz} region. In the negative R/L_{nz} region, the mode is driven by both impurity and electron density gradients. The results suggest that the observed electromagnetic turbulence could belong to a kind of drift instability which exhibits an electromagnetic feature. The electromagnetic turbulence can also be excited by externally seeded impurity in HL-2A [20]. HL-2A experimental results suggests that the quasi-stationary edge localized impurity profile offers the possibility to actively control the pedestal dynamics and ELMs via pedestal turbulence, which helps to protect plasma facing components.

2.2 Roles of Quasi-coherent Mode in Pedestal Dynamics and ELM Onset

The behaviors of pedestal pressure gradient collapse and rebuild in and after each ELM eruption have significant influence not only on plasma performance but also on in-vessel components such as first wall and divertor. Therefore, the dynamics of edge pedestal, including its formation and sustaining mechanisms such as plasma parameter evolutions in inter-ELM phases and triggering of ELMs in particular is under intensive investigation. In this regards, a few quasi-coherent modes quasi-coherent mode (QCMs) have been observed in the pedestal regions on tokamaks recently. All these results indicate that the modes observed induce out going particle or energy flow to limit further development of pressure gradient in the pedestal and avoid major explosive MHD activities and confinement degradation. A new QCM which was observed just prior to each ELM onset in H-mode plasmas on HL-2A tokamak. The mode induces an inward particle flux which contributes

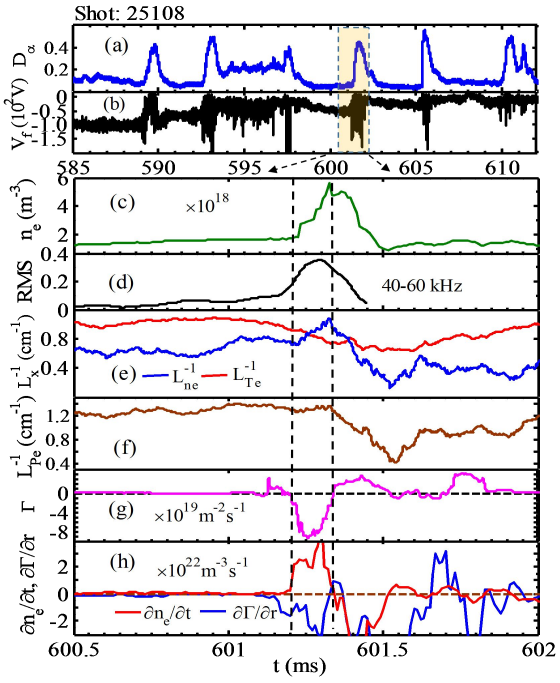

Figure 4. Evolutions of D_α emission (a), the fluctuation of floating potential (b), the local electron density (c), the root mean square of the floating potential fluctuation of 40-60 kHz (QCM) (d), the scale lengths of the electron temperature and density gradients (e), the scale length of plasma pressure gradient (f), the particle flux induced by the QCM (g), density derivative with respect to time and the divergence of the QCM induced particle flux (h).

significant additional density and its gradient/pressure gradient increase and may trigger the ELM onset.

Shown in Figures 4 (a) and (b) are the evolutions of D_α emission and floating potential fluctuations. It is not difficult to find that the amplitude of the floating potential fluctuation start to increases about 0.2 ms prior to each ELM onset. Actually, similar correspondences exist in quite a few physics quantities. In order to show such behaviors more clearly zoomed in plots are given in the left figures for one ELM. Figure 4(h) presents the QCM induced inward (negative) particle flux which is in good coincidence with the increases of to density (c) and its gradient (e). The time derivative of the density and the divergence of the QCM induced particle flux are given in (g). It is clearly shown that the QCM induced particle flux makes a significant contribution to the local particle balance and increment. The heat flux induced by the QCM is found to be negligible in the energy balance. The contribution from the QCM induced inward particle flux is one third of the total particle increment. It is important to point out that the phenomena are very similar prior to each ELM onset.

3. ELM Mitigation and Control

Various ELM mitigation or control techniques have been explored in HL-2A, including LHW, impurity seeding, RMP, SMBI and pellet injection. ELM mitigation experiments by using new LHW system with the PAM have been performed in HL-2A.The mitigation effect was synchronized with the increase of the pedestal turbulence measured by Doppler reflectometry. The ELM mitigation has been achieved by externally seeded impurities by means of laser blow-off (LBO) and SMBI systems.With SMBI technique, the experimental results indicated that the shallow deposition of SMBI is sufficient for ELM mitigation [10, 21]. ELM mitigation by applying n = 1 resonant magnetic perturbation was first obtained in recent HL-2A experiments. It was found that the ELM mitigation window is q_{95} = 3.65-3.85.

3.1 ELM Mitigation with LHCD

Recently LHCD has been shown to be a new method for ELM mitigation. ELM mitigation experiments with LHCD have been performed in HL-2A.Figure 5 shows the typical results. The ELM mitigation is characterized by the increase of the ELM frequency (Fig.5d) and the decrease of the ELM amplitude (Figs.5c and 5d). Comparing the LHCD antenna gas puff signal in Fig.5b with Figs.5c, 5d and 5e, we can conclude that the mitigation effect should not be due to the gas puff from the LHCD antenna, which is designed for improving the coupling of LHW to the plasma when the gap between the plasma and the LHCD antenna mouth is large.

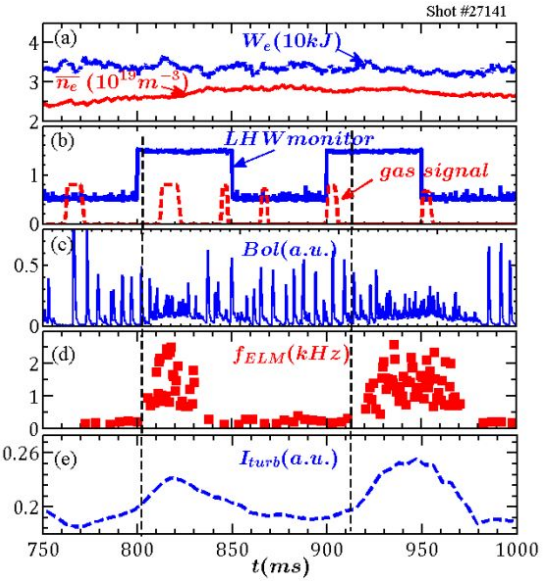

Figure.5 Time trace of the line-averaged density (red solid line)and the plasma stored energy （blue dashed line ） (a), the LHCD antenna gas puff signal(red dashed line)and the LHW monitoring (blue solid line)(b), the radiation measured by bolometer (c), the ELM frequency (d),and the intensity of the inter-ELM turbulence (e)

The image of infrared camera has shown that the divertor heat load released by ELM has been significantly reduced during the mitigation. The mitigation effect with LHCD has also been found to be very sensitive to the parameters as the plasma density and the LWH absorbed power. The desynchronization between LHCD pulse and the ELM mitigation shows that LHCD is only an indirect cause of the mitigation as shown in Figure 5. On the other hand, as shown in Figs.5d and 5e, the mitigation effect is synchronized with the increase of the pedestal turbulence measured by Doppler reflectometry, showing that the enhancement of the particle transport due to the pedestal turbulence could be the direct cause of the ELM mitigation.

3.2 ELM Mitigation by Injected Impurity Deposited in Pedestal

In recent HL-2A experiments, the ELM mitigation has been achieved by impurities externallyseeded by laser blow-off (LBO) and SMBI systems. Figure 6 illustrates the time evolution of the main parameters of one discharge with ELM mitigation. Impurity tungsten was injected into the plasma at t = 900ms. Following the impurity injection, the ELM frequency becomes higher while the amplitude becomes lower, implying that ELMs are mitigated. No obvious degradation of the confinement was observed during the ELM mitigation phase. The information of the impurity deposition can be given by the bolometer arrays. The impurity particles can penetrate the edge plasma and were mainly deposited in the pedestal region. The density fluctuations during ELM mitigation phase were significantly increased (as shown in figure 6d), showing that ELM mitigation is strongly correlated to the enhanced transport induced by turbulence in the pedestal. Thus the ELM mitigation may be achieved by the transport enhancement due to the impurity deposition in the pedestal.

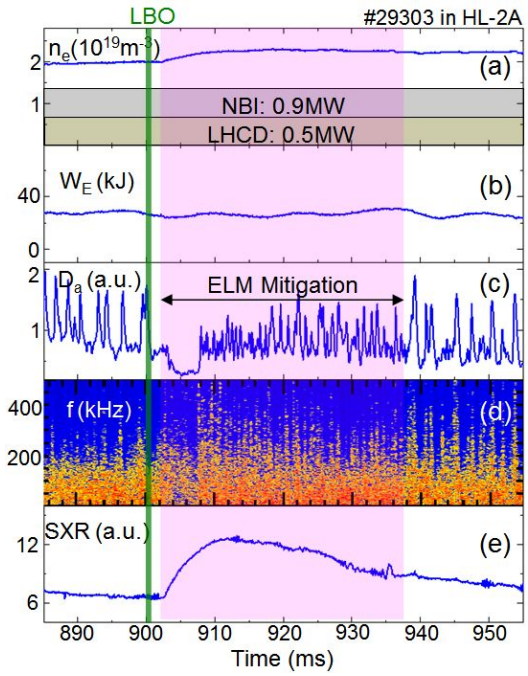

Figure 6. Time evolution of the main parameters of an H-mode discharge with ELM mitigation. (a) Electron density, (b) plasma stored energy, (c) divertor Da signal, (d) density fluctuation power spectra in pedestal top, (e) soft x-ray emission intensity. The shaded region represents the ELM-mitigation phase.

4. Core Plasma Transport

For the progress in core plasma transport, the iITBs were observed in the NBI heated plasmas. The results indicated the importance of flow shear on ITB sustainment [11].The effect of ECRH on the impurity transport has been investigated. The reduction of impurity concentration in the plasmas core was observed when the ECRH power deposited inside the sawtooth reversion surface [15].The tungsten spectra have been investigated in extreme ultraviolet (EUV) wavelength range. Two isolated line emissions were found in the low temperature plasma phase. A quasi-coherent TEM in spectra of density fluctuations has been

observed by multi-channel microwave reflectometers. The turbulence transition and the direct effect of the TEM on particle transport have been studied [13]. For non-local heat transport, it was found that the critical values of β to induce the NTMs in nonlocal discharges were substantially lower than those without nonlocal transport [14].A new-type nonlocal transport triggered by the ion fishbone was observed [12]. These findings revealed the dynamic interaction between turbulence and large-scale mode structures.

4.1 Ion Internal Transport Barriers

The ion internal transport barriers (iITBs) were observed in the NBI heated plasmas on the HL-2A tokamak [11]. The position of the barrier foot, in the stationary state, coincides with the q=1 flux surface within its uncertainty of measurement. The ion temperature and toroidal rotation profiles are shown in figure 7. For these shots with ITB, long lasting modes (fishbone oscillations) were observed during the peaked ion temperature and velocity phases. Another interesting observation is that the $T_i(0.5)$ in the discharges without iITBs seems not lower than that with iITBs; and it is clear that the $T_i(0.5)$ declines when the maximum R/L_{Ti} is higher than 14. Further analysis indicates that the $R/L_{Ti}(0.2)$ increases with $R/L_{Ti}(0.5)$ for the discharges without iITB. *W*hen the $R/L_{Ti}(0.2)$ is higher than 14, the iITB is formed. The characters of ion thermal diffusivity indicate that there is a typical ITB in the region ρ<0.4 before ECRH phase. During the ECRH phase without iITB, the $\chi_i$is higher and can be up to ~8 m^2/s. The iITB are observed only in discharges of $T_i \geq T_e$, and are not otherwise, indicating that the temperature ratio plays a very important role in the iITB formation.

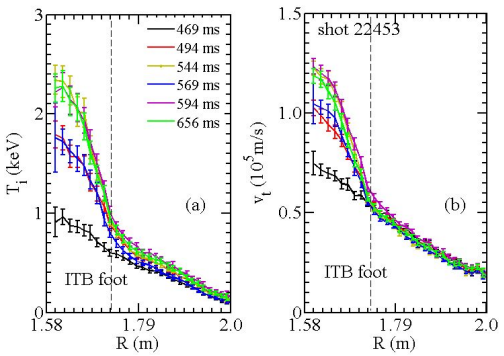

Figure 7. *T_i (a) and v_t (b) profiles.*

The drift turbulence is analyzed with HD7 code and the results indicate that the ITG mode turbulence is dominant for the peaked ion temperature discharges. Providing $E_r \approx v_t B_\theta$, the growth rate of ITG mode is lower than the shearing rate of the flow ($\omega_{E\times B}$) for the whole iITB region, indicating the importance of flow shear on ITB sustainment.

4.2Impurity Transport in ECRH Plasmas

The effect of ECRH on the impurity transport has been investigated with relation to the ECRH power deposition in the HL-2A tokamak [15]. The reduction of impurity concentration in the plasmas core was observed when the ECRH power deposited inside the sawtooth reversion surface. The reversed sawtooth oscillation in the central channels of the soft X ray (SXR) was observed while the normal sawtooth appears at the edge channels of the SXR. There was no such reversed sawtooth on the central SXR signal with the ECRH power deposited outside the sawtooth reversion surface. Based on the trace impurity injection with the laser blow-off technique, the impurity transport coefficients were estimated with a one dimensional impurity transport code STRAHL. Both diffusion coefficient D and convection velocity V are increased when the ECRH deposition position shifts inside the sawtooth inversion surface. The V has been greatly reversed to the outward direction with the inner-deposited ECRH but it normally directs inwards in the ohmic discharges. The outward flux of impurity can be significantly enhanced with the inner-deposited ECRH. The

calculated Al density profile also confirms that the central peaked impurity density profile has been effectively flattened with the inner-deposited ECRH. During the occurrence of the long-lasting m/n=1/1 mode an outward heat flux has been observed by the ECE measurement.

5. MHD and Energetic Particle Physics

Recently, the behaviors of runaway currents in MGI induced disruptions have been intensively investigated [16]. It was found that the SMBI can suppress the runaway current. The real-time (RT) control of NTMs by ECRH with launcher mirror steering has been developed on HL-2A. The stabilization of tearing modes with the ECRH feedback has been realized. In ohmic plasmas with weak magnetic shear and low pressure gradients, low-n Alfvenic ion temperature gradient (AITG) modes have been observed and identified [17]. Strong resonant and non-resonant internal kink modes were observed. Double m/n=1/1 e-fishbone modes propagating in the opposite directions poloidally were directly observed with the advanced 2D ECEI system in reversed magnetic shear plasma.

5.1 Mitigation of Runaway Current with SMBI

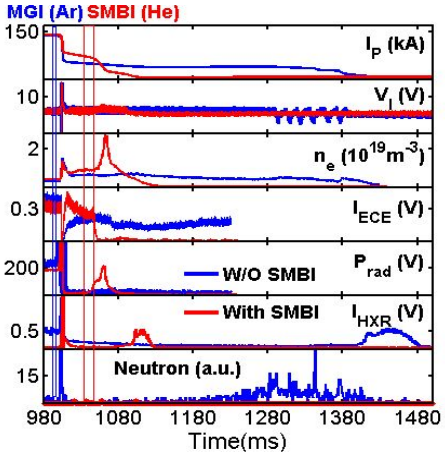

Figure 8 The disruption was triggered by MGI with Ar gas, and then the runaway current was mitigated by using SMBI to inject He gas.

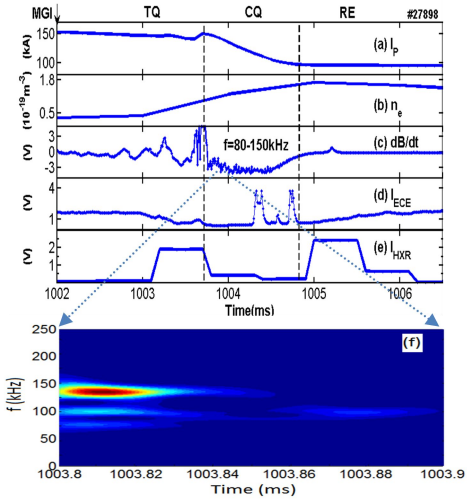

Figure 9. (a) Time traces in the current quench phase showing plasma current I_P, (b) electron density n_e, (c) magnetic instability dB/dt, (d) radiation of Electron Cyclotron Emission I_{ECE}, (e) hard x-ray radiation I_{HXR} and (f) spectrogram of Mirnov signal.

Dedicated experiments have been carried out with the SMBI combined with the MGI on HL-2A [16]. The behaviors of runaway currents in MGI induced disruptions have been investigated. Long-lasting runaway electron (RE) plateau was achieved after argon injection by MGI even at B_t = 1.28 T, much lower than previous B_t threshold found in other tokamaks. It was found that argon injection can cause the generation of runaways carrying up to 30% of the initial plasma current. Moreover, the runaway current caused by argon injection with MGI was successfully suppressed by SMBI with a number of injected atoms of about 1.0×10^{21}, as shown in Figure 8. Light gases, such as helium, are selected in this experiment for its high efficiency in increasing the density. These experiments suggest that SMBI might be viable for runaway suppression in future tokamaks.In addition, a toroidal alfvén eignmode (TAE) -like instability was observed during disruptions deliberately triggered by MGI of argon as shown in Figure 9. This mode occurs at

the beginning of the current quench and lasts about 1-2 ms. These instabilities appears to be favorable in limiting the RE beam formation. It has been found that the runaway plateau is easy to obtain on the condition of high normalized magnetic fluctuation level($\delta B/B_T$), the runaway plateau is even invisible when $\delta B/B_T$ the exceeds the threshold of about 7.8×10^{-4}, indicating that this magnetic mode plays a scattering role on the RE beam strength.

5.2Real-time Control of Tearing Modes with ECRH

The RT control of NTMs by ECRH with launcher mirror steering has been developed on HL-2A. A few RT diagnostics and intelligent controllers achieved precise control of ECRH deposition at a rational surface. A reliable feedback loop has been designed, developed and tested by a proper integration and coordination of several diagnostic systems with plasma control system (PCS). An RT code solves Grad-Shafranov equation with 129 × 129 grid scale using the advanced parallel computation within 1 ms. The magnetic island location was determined by the RT 'ECE/Mirnov' subsystem with the high spatial resolution less than 1 cm. Motor controller will calculate the control signal with all the possible signals from the reflective memory networking. The stabilization of tearing modes with the ECRH feedback has been demonstrated on HL-2A, as shown in figure 10.

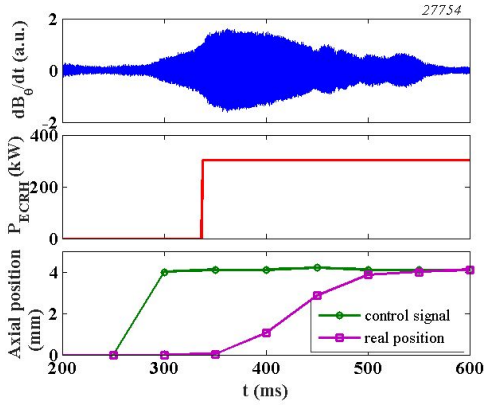

Figure 10. Real time control of tearing mode.

5.3 Low-n Alfvenic Ion Temperature Gradient Modes and Internal Kink Modes

Low-n Alfvenic ion temperature gradient (AITG) modes have been observed and identified in HL-2A ohmic plasmas with weak magnetic shear $(s\sim0)$ and low pressure gradients $(\alpha<0.3)$ [17]. A group of oscillations with f=15-40 kHz and n=3-6 is detected by various diagnostics in high-density ohmic regimes, and it is shown in Fig.11. It was suggested that the modes were excited by pressure gradients. The time trace of the fluctuation spectrogram can be either a frequency staircase, with different modes excited at different times or multiple modes may simultaneously coexist. Theoretical analyses by the extended generalized fishbone-like dispersion relation (GFLDR-E) reveal that the mode frequencies scale with ion diamagnetic drift frequency and η_i, and they lie in KBM-AITG-BAE frequency ranges. AITG modes are most unstable when the magnetic shear is small in low pressure gradient

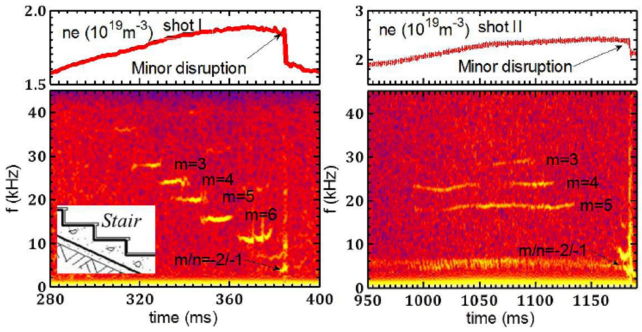

Figure 11. Typical discharges with AITG activities on HL-2A. 2D patterns are spectrograms of ECEI (left) and soft X-ray signal. Left col.(shot I, Bt=1.31T, Ip=150kA) with the frequency staircase; Right col.(shot II, Bt=1.35T, Ip=150kA) with the multi-mode coexistence.

regions. It is worth emphasizing that these instabilities may be linked to the internal transport barrier (ITB) and H-mode pedestal physics for weak magnetic shear. Strong resonant and non-resonant internal kink modes, abbreviated as RKs and NRKs, are observed. The RK has characteristics of periodic strong bursting amplitude and rapid chirping-down frequency, but the NRK usually has the saturated amplitude, slow changed or constant frequency and long-lasting time. The NRK excited by energetic electrons is found for the first time. These modes poloidally propagate in electron diamagnetic directions.

6. Edge Turbulence

For the first time, the synchronization of GAMs and magnetic fluctuations in the edge plasmas was observed. The frequency entrainment and phase lock were also elucidated [18]. Three-dimensional structures of zonal flows have been studied by using multi-channel correlation Doppler reflectometers. In addition, theoretical predictions of Landau damping and collisional damping for the GAM amplitude were demonstrated [19]. The mechanisms for the generation of blobs/holes at the boundary have been investigated [22].

6.1 Synchronization of GAMs and Magnetic Fluctuations

The synchronization of GAMs and magnetic fluctuations in the edge plasmas of the HL-2A tokamak was observed for the first time [18]. The frequency entrainment and phase lock were also elucidated. The meso-scale electrostatic fluctuations (MSEFs) at frequency of ~10.5 kHz with components of the dominant GAMs (n = 0) and the m/n = 6/2 potential fluctuations were detected inside the last closed flux surface (LCFS) in ECRH plasmas using multiple Langmuir probe arrays, as shown in figure 12(a). The small peak in figure 12(b) at the same frequency as the MSEFs has the components of the dominant m/n = 6/2 magnetic fluctuations and the zonal field (n = 0), besides the main peak of m/n = 2/1 appears at ~6 kHz. The bicoherence analysis suggests that the MSEFs may contribute to the low frequency zonal flow (LFZF) formation through the nonlinear three wave coupling between LFZFs and MSEFs. Their summed bicoherence, shown in figure 12(d), indicate that LFZFs and MSEFs can also interact with the turbulence. Experimental results also suggest that the phase shifts between the GAMs and magnetic fluctuations are locked through adjusting their phases via nonlinear interaction.

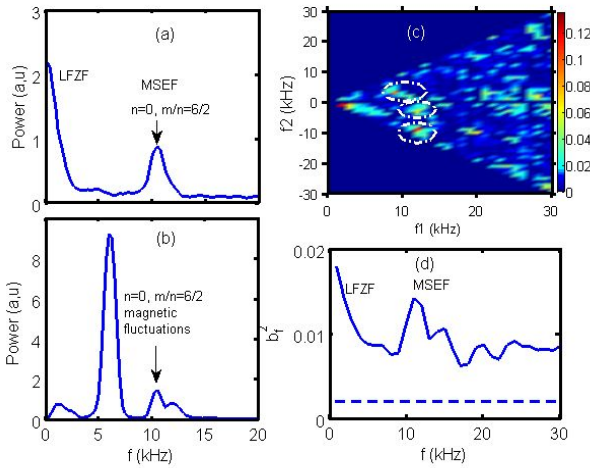

Figure 12. The auto-power spectra of the floating potential fluctuations (a), magnetic fluctuations (b), squared bicoherence (c), summed bicoherence (d).

6.2 Zonal Flows Studied by Multi-channel Correlation Doppler Reflectometry

Recently, the microwave reflectometry, especially the Doppler reflectometry has been developed and improved significantly in the HL-2A tokamak [6]. Specifically, the oscillations of poloidal plasma flows induced by radially sheared zonal flows were investigated by multi-channel correlation Doppler reflectometers [19]. With poloidally and toroidally

equipped Doppler reflectometry, the long range correlation of E_r can be measured. The poloidal and toroidal cross power and phase spectra of E_r fluctuations are shown in figure 13a and 13b. The phase shifts are near zero, demonstrating the two dimensional symmetry (m = 0 and n = 0) of GAM in the electric field fluctuation component. The GAM is believed to be driven by turbulent Reynolds stress by nonlinear three wave interaction. To demonstrate the process, the squared auto-bicoherence of the E_r fluctuations was calculated and shown in figure 13c. The result indicates that the nonlinear three wave interaction is responsible for the generation of the GAM. Its acoustic property in radial direction was also studied. The coexistence of LFZF and GAM was found. In addition, theoretical predictions of Landau damping and collisional damping for the GAM amplitude were demonstrated.

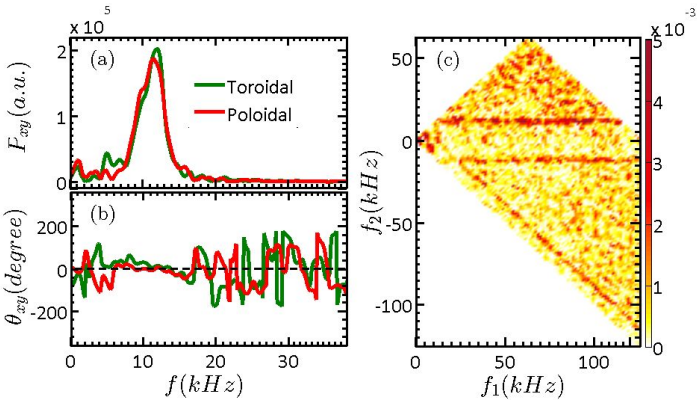

Figure 13. (a) Poloidal and toroidal cross-power spectra of E_r fluctuations between two separated ports and (b) corresponding cross-phase spectra,the distance of two poloidally separated antennas is about 0.3 m. In toroidal direction, the distance is about 1.5 m. (c) Squared bicoherence spectrum of the E_r fluctuations.

7. Summary

Since the 2014 Fusion Energy Conference, the HL-2A tokamak has achieved significant progress in the studies of H-mode physics, ELM mitigation and control, core plasma transport, MHD and energetic particle physics, and edge turbulence. Double critical impurity gradient of electromagnetic turbulence was observed in the H-mode plasmas. This result suggests that the quasi-stationary edge localized impurity profile offers the possibility to actively control the pedestal dynamics and ELMs via pedestal turbulence, which helps to protect plasma facing components. A new QCM was observed just prior to each ELM onset. The mode induces an inward particle flux which contributes significant additional density and its gradient/pressure gradient increase and may trigger the ELM onset. ELM mitigation and control has achieved by SMBI, impurity seeding, RMP and LHW. The ion internal transport barrier was observed in the NBI heated plasmas. The results suggested the importance of flow shear on ITB sustainment. NTMs driven by the transient perturbation of local electron temperature during the non-local thermal transport events have been observed, and a new-type nonlocal transport triggered by the ion fishbone was observed. These findings revealed the dynamic interaction between turbulence and large-scale mode structures. Long-lasting RE plateau was achieved after argon injection by MGI even at B_t = 1.28 T, much lower than previous B_t threshold found in other tokamaks. And the runaway current was successfully suppressed by SMBI. In addition, a TAE-like instability was observed during disruptions deliberately triggered by MGI. It was found that low-n AITG modes (f=15-40 kHz and n=3-6) can be excited in ohmic plasmas with weak magnetic shear and low pressure gradients. Strong resonant and non-resonant internal kink modes were observed in high-power ECRH+ECCD plasmas. For the first time, the synchronization of GAMs and magnetic fluctuations was observed in the edge plasmas. The frequency entrainment and phase lock were also elucidated.

Spatiotemporal features of zonal flows have been studied by using multi-channel correlation Doppler reflectometers.

Acknowledgment

The authors would like to acknowledge all those who have contributed to the HL-2A projects, and are particularly thankful to M. Kikuchi and A. Bécoulet for useful discussion and comments, and the colleagues of IRFM at CEA in France for their dedicated contribution to the HL-2A LHCD system.

References

[1] Bai X.Y. *et al.,* Proc. 42nd EPS Conference on Plasma Physics, Lisbon (2015), P5.137.

[2] Ekedahl, A., *et al.,* 2016 [EX/P7-34] paper presented at the *26th IAEA Conf. on Fusion Energy (Kyoto, Japan)*.

[3] Li Y.G. *et al,*2016 *JINST***11**C02002.

[4] Zhou Y. *et al,*2016 *Rev.Sci. Instrum.* **87**,11E,107.

[5] Jiang M. *et.al,*2015 *Rev. Sci. Instrum*. **83**,10E,336.

[6] Zhong W.L.*et al.,* 2015 *JINST* **10**, P10014.

[7] Xu Yuan *et al.,*2016*Rev. Sci. Instrum*. **87**, 023507 .

[8] Zhong W.L. *et al.,* 2016 *Phys. Rev. Lett.***117**, 045001.

[9] Dong J.Q. *et al.,*2016 [EX/P7-24] paper presented at the *26th IAEA Conf. on Fusion Energy (Kyoto, Japan)*.

[10] Shi Z.B. *et al.,*2016 [EX/P7-22] paper presented at the *26th IAEA Conf. on Fusion Energy (Kyoto, Japan)*.

[11] Yu D.L. *et al.,*2016 [EX/8-2] paper presented at the *26th IAEA Conf. on Fusion Energy (Kyoto, Japan)*.

[12] Chen W. *et al.,*2016 *Nucl. Fusion* **56** 044001.

[13] Zhong W.L. *et al.,*2016 *Phys. Plasmas* **23**, 060702 .

[14] Ji X. Q. *et al.,* 2016[EX/P7-19] paper presented at the *26th IAEA Conf. on Fusion Energy (Kyoto, Japan)*.

[15] Cui Z.Y *et al.,* 2016 [EX/P7-21] paper presented at the *26th IAEA Conf. on Fusion Energy (Kyoto, Japan)*.

[16] Liu Yi *et al.,*2016 [EX/9-3] paper presented at the *26th IAEA Conf. on Fusion Energy (Kyoto, Japan)*.

[17] Chen W. *et al.,*2016 [EX/P7-17] paper presented at the *26th IAEA Conf. on Fusion Energy (Kyoto, Japan)*.

[18] Yan L.W. *et al.,*2016 [EX/P7-27] paper presented at the *26th IAEA Conf. on Fusion Energy (Kyoto, Japan)*.

[19] Zhong W.L. *et al.,* 2015 *Nucl. Fusion* **55** 113005.

[20] Zhong W.L. *et al* 2016 *43rd EPS conference of Plasma Physics* Leuven, Belgium, I5.118

[21] Yang Z.C. *et al* 2016 *Phys. Plasmas* **23** 012515

[22] Xu Y. *et al.,*2016 [EX/P7-29] paper presented at the *26th IAEA Conf. on Fusion Energy (Kyoto, Japan)*.